We are IntechOpen, the world's leading publisher of Open Access books Built by scientists, for scientists

6,900
Open access books available

185,000
International authors and editors

200M
Downloads

Our authors are among the

154
Countries delivered to

TOP 1%
most cited scientists

12.2%
Contributors from top 500 universities

WEB OF SCIENCE™

Selection of our books indexed in the Book Citation Index in Web of Science™ Core Collection (BKCI)

Interested in publishing with us?
Contact book.department@intechopen.com

Numbers displayed above are based on latest data collected.
For more information visit www.intechopen.com

5

Ferrofluid Seals

V. Lemarquand[1] and G. Lemarquand[2]
[1]*LAPLACE UMR CNRS 5213, IUT Figeac, Universite de Toulouse, Avenue de Nayrac, 46100 Figeac*
[2]*Laboratoire d'Acoustique de l'Universite du Maine UMR CNRS 6613, Avenue Olivier Messiaen, 72085 Le Mans Cedex 9*
France

1. Introduction

Ferrofluids are very peculiar materials. Indeed, a stable colloidal suspension of magnetic particles in a liquid carrier is something special. These magnetic particles, of about 10 nanometers in diameter, are coated with a stabilizing dispersing agent that prevents their agglomeration. The liquid can be either water or synthetic hydrocarbon or mineral oil. But this material class, discovered in the 1960s, proves specific various chemical and physical properties, whose increasing knowledge leads to ever more numerous technological applications.

Indeed, they are efficiently used in various engineering areas such as heat transfers, motion control systems, damping systems (1), sensors (2)(3). Their use to design fluid linear pumps for medical applications seems also very promising (4)(5). However, they are more commonly used as squeeze films in seals and bearings for rotating devices. Tarapov carried out some pioneering work regarding the ferrofluid lubrication in the case of a plain journal submitted to a non-uniform magnetic field (6) but more recent works show and discuss the recent trends in such a use (7)-(13). Moreover, ferrofluid dynamic bearings have been regularly studied and their static and dynamic characteristics have been described theoretically (14)-(21).

The various properties of ferrofluids enable them to fulfill such functions as heat transfer, ensuring airtightness, working as a radial bearing. Therefore they are used in electrodynamic loudspeakers. Moreover, a ferrofluid seal can replace the loudspeaker suspension and leads to a better linearity of the emissive face movement (22)-(26). This chapter intends to explain how ferrofluid seals are formed in magnetic structures by presenting a simple analytical model to describe their static behavior (27)(28). The originality lies in the fact that the considered structures are made of permanent magnet only, without any iron on the static part. The moving part is a non magnetic cylinder. The seal shape and performances are described with regard to the magnetic structure. The evaluation of the seal static capacity is given. Moreover, the seal shape changes when the seal is radially crushed by the inner cylinder: these changes are described and calculated and the radial force exerted by the ferrofluid on the moving part is determined as well as the stiffnesses associated.

Then, various magnetic structures are presented and studied to illustrate the magnet role and deduct some design rules for ferrofluid seals with given mechanical characteristics.

2. Structure and method description

This section presents the basic ironless structure used to create a magnetic field which has the double function of trapping and fixing the ferrofluid to form a seal.
The device is cylindrical and constituted of a static outer part made of stacked ring permanent magnets separated from the inner non magnetic moving part by an airgap. The number of ring magnets is an issue and will be discussed later on. The simplest structure has a single ring, but the performances are better for two or three rings, and even more, depending on the intended values. The magnet polarization direction is also an issue and can be either axial or radial. The trick may be to associate correctly two kinds of polarization.
The ferrofluid is located in the airgap and forms a seal between the moving and the static parts.

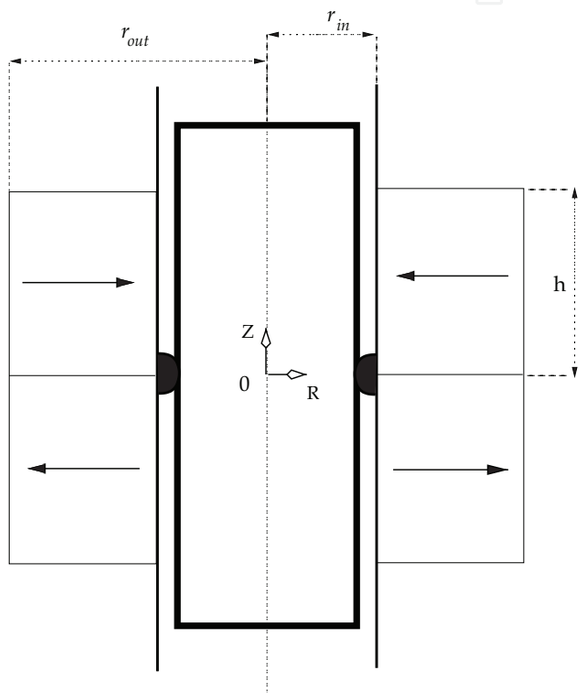

Fig. 1. Geometry : two outer ring permanent magnets and an inner non-magnetic cylinder with a ferrofluid seal between them; the ring inner radius is r_{in}, the ring outer radius is r_{out}, the height of a ring permanent magnet is h.

The ring inner radius is r_{in}, the ring outer radius is r_{out} and the ring permanent magnet height is h. The z axis is a symmetry axis.
The first step of the modelling is to calculate the magnetic field created by the permanent magnets. Exact formulations for the three components of the magnetic field created by axially or radially polarized permanent magnets have been given in the past few years. They are based either on the coulombian model of the magnets or their amperian one. Both models are equivalent for the magnet description but aren't for calculating: one may be more adapted to lead to compact formulations in some configurations where the other will be successful in others. The calculations of this chapter were carried out with formulations obtained with the coulombian model of the permanent magnets.
The location and the shape of the ferrofluid seal will be deducted from the magnetic field value by energetic considerations. Nevertheless, the conditions of use of the ferrofluid have to be

given here, as they differ from the ones encountered in their usual applications. Indeed, the magnetic field created by the magnets, which are considered to be rare earth ones (and rather Neodymium Iron Boron ones), is higher than 400 kA/m and the ferrofluid is consequently saturated, as the highest saturation field of the available ferrofluids are between 30 and 40 kA/m. This means that the field created by the ferrofluid itself won't really modifiy the total field and therefore it can be neglected. This is a great difference with most of the usual applications of the ferrofluids. Moreover, as the ferrofluid is completely saturated, its magnetic permeability is equal to one. Its magnetization is denoted M_s.
Furthermore, all the particles of the saturated ferrofluid are aligned with the permanent magnet field. So, the ferrofluid polarization has the same direction as the magnet orienting field. In addition, the sedimentation in chains of the ferrofluid particles is omitted (29).
Some other assumptions are made: the thermal energy, E_T, ($E_T = kT$ where k is Boltzmann's constant and T is the absolute temperature in degrees Kelvin) and the gravitational energy, E_G, ($E_G = \Delta\rho VgL$ where V is the volume for a spherical particle, L is the elevation in the gravitational field, g is the standard gravity, $\Delta\rho$ is the difference between the ferrofluid density and the outer fluid) are neglected. In addition, the surface tension exists but its effects can be omitted as the considering of both values of the surface tension coefficient, A, (A equals $0.0256 kg/s^2$ for the considered ferrofluids) and the radius of curvature leads to the conclusion that it won't deform the free boundary surface.
One of the aims of this chapter is to describe how the ferrofluid seals are formed and which is their shape. It has to be noted that the ferrofluid location depends on the value of the magnetic field in the airgap. Furthermore, the seal shape is the shape of the free boundary surface of the ferrofluid, which is a result of the competing forces or pressures on it. And the predominant pressure is the magnetic one. Therefore, the calculation of the magnetic field will be explained first and then the concept of magnetic pressure will be detailed.

3. Magnetic field calculation

3.1 Basic equations

The magnetic field created by the ring permanent magnets can be determined with a fully analytical approach. Let us consider the four fundamental Maxwell's equations:

$$\vec{\nabla}.\vec{B} = 0 \tag{1}$$

$$\vec{\nabla} \wedge \vec{H} = \vec{j} \tag{2}$$

$$\vec{\nabla}.\vec{D} = \rho \tag{3}$$

$$\vec{\nabla} \wedge \vec{E} = -\frac{\partial \vec{B}}{\partial t} \tag{4}$$

where $\vec{B}$ is the magnetic induction field, $\vec{H}$ is the magnetic field, $\vec{j}$ is the volume current density, $\vec{D}$ is the electric flux density, $\vec{E}$ is the electrostatic field and ρ is the electrical charge. The currents are nil in the considered structures as the magnetic field is created only by the permanent magnets. The vector fields $\vec{B}$ and $\vec{H}$ are defined for all points in space with the following relation:

$$\vec{B} = \mu_0 \vec{H} + \vec{J} \tag{5}$$

where μ_0 is the vacuum magnetic permeability and $\vec{J}$ is the magnet polarization. When the magnetic field is evaluated outside the magnet, $\vec{J} = \vec{0}$. The analogy with the Mawxell's

equations leads to write that:

$$\vec{\nabla}.\vec{H} = -\frac{\vec{\nabla}.\vec{J}}{\mu_0} = \frac{\sigma^*}{\mu_0} \tag{6}$$

where σ^* corresponds to a fictitious magnetic pole density. On the other hand, the magnetic field $\vec{H}$ verifies:

$$\vec{\nabla} \wedge \vec{H} = \vec{0} \tag{7}$$

Thus, $\vec{H}$ can be deducted from a scalar potential $\phi(\vec{r})$ by

$$\vec{H} = -\vec{\nabla}\left(\phi(\vec{r})\right) \tag{8}$$

For a structure with several ring permanent magnets, (6) and (7), lead to:

$$\phi(\vec{r}) = \frac{1}{4\pi\mu_0}\left(\sum_i \int\int_{S_i} \frac{\vec{J_k}.d\vec{S_i}}{\left|\vec{r}-\vec{r'}\right|} + \sum_j \int\int\int_{V_j} \frac{-\vec{\nabla}.\vec{J_k}}{\left|\vec{r}-\vec{r'}\right|} dV_j\right) \tag{9}$$

where $\vec{J_k}$ is the magnetic polarization of the k ring permanent magnet and $\left|\vec{r}-\vec{r'}\right|$ is the distance between the observation point and a magnetic charge contribution. Then the magnetic field created by the ring permanent magnets is determined as follows:

$$\vec{H} = -\vec{\nabla}.\left(\frac{1}{4\pi\mu_0}\left(\sum_i \int\int_{S_i} \frac{\vec{J_k}.d\vec{S_i}}{\left|\vec{r}-\vec{r'}\right|} + \sum_j \int\int\int_{V_j} \frac{-\vec{\nabla}.\vec{J_k}}{\left|\vec{r}-\vec{r'}\right|} dV_j\right)\right) \tag{10}$$

3.2 Magnetic field created by ring permanent magnets

The coulombian model of the magnets is used to determine the magnetic field created by the ring magnets (30)-(33). Moreover, the devices dimensions are supposed to be chosen so that the volume pole density related to the magnetization divergence can be neglected: the rings are assumed radially thin enough. Indeed, its influence has been discussed by the authors in some complementary papers.

Consequently, each permanent magnet is represented by two charged surfaces. In the case of a radially polarized permanent magnet the magnetic poles are located on both curved surfaces of the ring and the magnetic pole surface density is denoted σ^* (Fig. 2). In the case of an axially polarized permanent magnet, the magnetic pole surface density σ^* is located on the upper and lower faces of the ring (Fig. 3).

The three magnetic field components have been completely evaluated in some previous papers. As the structure is axisymmetrical, only two components of the magnetic field created by the magnets have to be evaluated: the axial one and the radial one, and they only depend on both dimensions z and r.

The radial component $H_r(r,z)$ of the magnetic field created by the permanent magnet is given by (11).

$$H_r(r,z) = \frac{\sigma^*}{\pi\mu_0} i(1+u)\left(\varsigma(u_1) - \varsigma(u_2)\right) \tag{11}$$

where the parameter i is the imaginary number $(i^2 = -1)$, with

$$
\begin{aligned}
\varsigma(u) \quad = \quad & \frac{\xi_1(-(a_1d+b_1(c+e_1)))F^*\left[i\sinh^{-1}[\frac{\sqrt{-c+d-e_1}}{\sqrt{c+e_1+du}}],\frac{c+d+e_1}{c-d+e_1}\right]}{d\sqrt{-c+d-e_1}e_1\sqrt{\frac{d(1+u)}{c+e_1+du}}\sqrt{1-u^2}} \\
& + \frac{\xi_1(b_1c-a_1d)\Pi^*\left[\frac{e_1}{c-d+e_1},i\sinh^{-1}[\frac{\sqrt{-c+d+e_1}}{c+e_1+du}],\frac{c+d+e_1}{c-d+e_1}\right]}{d\sqrt{-c+d-e_1}e_1\sqrt{\frac{d(1+u)}{c+e_1+du}}\sqrt{1-u^2}} \\
& + \frac{\xi_2\left(-(a_2d+b_2(c+e_2))\right)F^*\left[i\sinh^{-1}[\frac{\sqrt{-c+d-e_2}}{\sqrt{c+e_2+du}}],\frac{c+d+e_2}{c-d+e_2}\right]}{d\sqrt{-c+d-e_2}e_2\sqrt{\frac{d(1+u)}{c+e_2+du}}\sqrt{1-u^2}} \\
& + \frac{\xi_2(b_2c-a_2d)\Pi^*\left[\frac{e_2}{c-d+e_2},i\sinh^{-1}[\frac{\sqrt{-c+d+e_2}}{c+e_2+du}],\frac{c+d+e_2}{c-d+e_2}\right]}{d\sqrt{-c+d-e_2}e_2\sqrt{\frac{d(1+u)}{c+e_2+du}}\sqrt{1-u^2}} \\
& - \frac{\eta_3\left((a_3d-b_3e_3)\right)F^*\left[i\sinh^{-1}[\frac{\sqrt{-d-e_3}}{\sqrt{e_3+du}}],\frac{-d-e_3}{d+e_3}\right]}{d\sqrt{-d-e_3}(-c+e_3)\sqrt{\frac{d(1+u)}{e_3+du}}\sqrt{1-u^2}} \\
& - \frac{\eta_3(b_3c-a_3d)\Pi^*\left[\frac{-c+e_3}{d+e_3},i\sinh^{-1}[\frac{\sqrt{-d+e_3}}{e_3+du}],\frac{-d+e_3}{d+e_3}\right]}{d\sqrt{-d-e_3}(-c+e_3)\sqrt{\frac{d(1+u)}{e_3+du}}\sqrt{1-u^2}} \\
& - \frac{\eta_4\left(a_4d-b_4e_4\right)F^*\left[i\sinh^{-1}[\frac{\sqrt{-d-e_4}}{\sqrt{e_4+du}}],\frac{-d+e_4}{d+e_4}\right]}{d\sqrt{-d-e_4}(c+e_4)\sqrt{\frac{d(1+u)}{e_4+du}}\sqrt{1-u^2}} \\
& - \frac{\eta_4(b_4c-a_4d)\Pi^*\left[\frac{-c+e_4}{d+e_4},i\sinh^{-1}[\frac{\sqrt{-d-e_4}}{e_4+du}],\frac{-d+e_4}{d+e_4}\right]}{d\sqrt{-d-e_4}(-c+e_4)\sqrt{\frac{d(1+u)}{e_4+du}}\sqrt{1-u^2}}
\end{aligned}
\tag{12}
$$

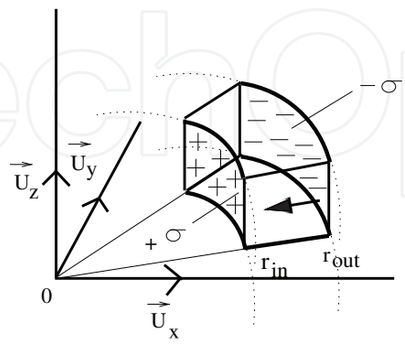

Fig. 2. Radially polarized tile permanent magnet: the inner curved face is charged with the magnetic pole surface density $+\sigma^*$ and the outer curved face is charged with the magnetic pole surface density $-\sigma^*$, the inner radius is r_{in}, the outer one is r_{out}

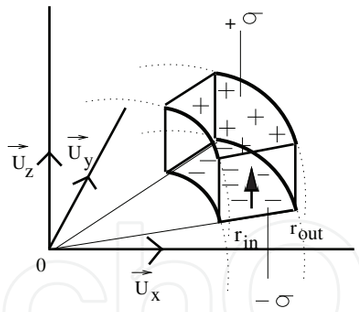

Fig. 3. Axially polarized tile permanent magnet: the upper face is charged with the magnetic pole surface density $+\sigma^*$ and the lower face is charged with the magnetic pole surface density $-\sigma^*$, the inner radius is r_{in}, the outer one is r_{out}

The axial component of the magnetic field created by the ring permanent magnet is given by (13).

$$\begin{aligned} H_z(r,z) &= \frac{\sigma^*}{\pi\mu_0}\left(-r_{in}\frac{K^*\left[\frac{-4rr_{in}}{(r-r_{in})^2+z^2}\right]}{\sqrt{(r-r_{in})^2+z^2}}\right) \\ &+\frac{\sigma^*}{\pi\mu_0}\left(r_{in}\frac{K^*\left[\frac{-4rr_{in}}{(r-r_{in})^2+(z-h)^2}\right]}{\sqrt{(r-r_{in})^2+(z-h)^2}}\right) \\ &-\frac{\sigma^*}{\pi\mu_0}\left(r_{in}\frac{K^*\left[\frac{-4rr_{in}}{(r-r_{in})^2+z^2}\right]}{\sqrt{(r-r_{in})^2+z^2}}\right) \\ &+\frac{\sigma^*}{\pi\mu_0}\left(r_{in}\frac{K^*\left[\frac{-4rr_{in}}{(r-r_{in})^2+(z+h)^2}\right]}{\sqrt{(r-r_{in})^2+(z+h)^2}}\right) \end{aligned} \tag{13}$$

$$\xi_i = \sqrt{\frac{d(-1+u)}{c+e_i+du}} \tag{14}$$

$$\eta_i = \sqrt{\frac{d(-1+u)}{e_i+du}} \tag{15}$$

where $K^*[m]$ is written in terms of the incomplete elliptic integral of the first kind by (16)

$$K^*[m] = F^*[\frac{\pi}{2}, m] \tag{16}$$

$F^*[\phi, m]$ is written in terms of the elliptic integral of the first kind by (17):

$$F^*[\phi, m] = \int_{\theta=0}^{\theta=\phi} \frac{1}{\sqrt{1-m\sin(\theta)^2}} d\theta \tag{17}$$

Parameters	
a_1	$r_{in}rz$
b_1	$\text{-}r_{in}^2 z$
c	$r^2 + r_{in}^2$
d	$-2rr_{in}$
e_1	z^2
a_2	$-r_{in}r(z-h)$
b_2	$r_{in}^2(z-h)$
e_2	$(z-h)^2$
a_3	$r_{in}rz$
b_3	$-r_{in}^2 z$
e_3	$r^2 + r_{in}^2 + z^2$
a_4	$r_{in}r(-z-h)$
b_4	$-r_{in}^2(-z-h)$
e_4	$r^2 + r_{in}^2 + (z+h)^2$

Table 1. Definition of the parameters used in (12)

$\Pi^*[n,\phi,m]$ is written in terms of the incomplete elliptic integral of the third kind by (18)

$$\Pi^*[n,\phi,m] = \int_0^{\phi} \frac{1}{(1-n\sin(\theta)^2)\sqrt{1-m\sin(\theta)^2}} d\theta \tag{18}$$

The parameters used in (12) are defined in Table 1. As a remark, an imaginary part, which has no physical meaning, may appear because of the calculus noise of the calulation program (Mathematica). Therefore, the real part only of $H_r(r,z)$ must be considered.

4. The magnetic pressure

The magnetic pressure determines the shape of the free boundary surface of the ferrofluid. Moreover, the assumptions for the calculations have been described in the method description section (2).
Then, the magnetic pressure is defined as follows:

$$p_m(r,z) = \mu_0 \mathbf{M_s}.\vec{H}(r,z) = \mu_0 M_s \sqrt{H_r(r,z)^2 + H_z(r,z)^2} \tag{19}$$

where the evaluation of both magnetic field components $H_r(r,z)$ and $H_z(r,z)$ have been given in the previous section and where M_s is the magnetization of a magnetic particle of the ferrofluid. Thus, the magnetic pressure is the interaction of the magnetic field created by the permanent magnets and the particle magnetization. Eventually, for hydrodynamic pressures which equal zero or have low values, the seal free boundary surface is a magnetic iso-pressure surface.
Fig. 4 shows a three-dimensional representation of the magnetic pressure created by two in opposed directions radially polarized ring permanent magnets. This magnetic pressure can also be seen as a magnetic energy volume density, and can be given either in N/m^2 or in J/m^3.

The magnetic pressure $p_m(r,z)$ has been evaluated with (19). Figure 4 shows that the magnetic pressure is higher next to the ring magnets, especially where both the magnetic field and its gradient are the strongest.

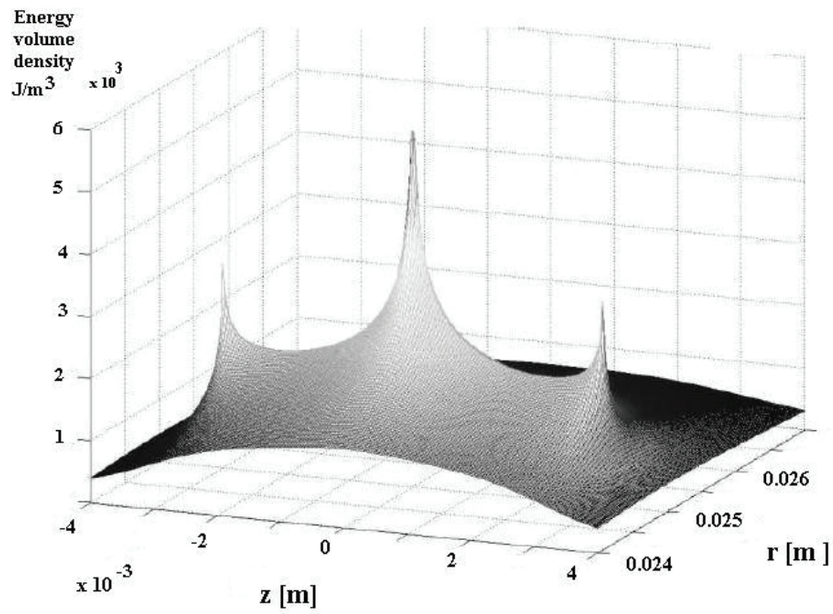

Fig. 4. Three-dimensional representation of the magnetic pressure in front of two in opposed directions radially polarized ring permanent magnets.

This representation also shows that the potential energy is concentrated in a very small ferrofluid volume. As a consequence, it gives information on what quantity of ferrofluid should be used to create a ferrofluid seal. When a large quantity of ferrofluid is used, then the ferrofluid seal is thick and the potential energy increases. But the viscous effects become an actual drawback with regard to the dynamic of the inner moving cylinder. When too small an amount of ferrofluid is used, then the viscous effects disappear but the main properties of the ferrofluid seal (damping, stability, linearity,...) disappear as well. So, an adequate quantity of ferrofluid corresponds to a given geometry (here two ring permanent magnets with an inner non-magnetic cylinder) in order to obtain interesting physical properties with very little viscous effects.
The concept of potential energy thus appears, which is defined by (24):

$$E_m = -\int\int\int_{(\Omega)} p_m(r,z)dV \tag{20}$$

where (Ω) is the ferrofluid seal volume. Indeed, this potential energy, given in J, allows the calculation of the seal mechanical properties and will be used throughout the remainder of this chapter.

5. Shape of the ferrofluid seal

As the shape of the seal depends on the magnetic pressure in the structure it naturally depends on the magnetic structure which creates the magnetic field. This section intends to describe some structures and discuss the corresponding seals.

5.1 Basic structure

Figure 5 shows the structure constituting the base of all the devices presented. It consists of three outer stacked rings, of an inner non-magnetic piston and of ferrofluid seals. The

piston is radially centered with the rings. The rings' inner radius, r_{in}, equals 25 mm and their outer radius, r_{out}, equals 28 mm. The rings can be either made with permanent magnet -as here the middle ring- or with non-magnetic material -like the upper and lower rings-. The ferrofluid seals are located in the air gap between the piston and the rings. The whole section will discuss the seal number, their position and the polarization direction of the ring magnets. Furthermore, the radial component of the magnetic field created by the ring permanent magnets is also presented for each studied configuration in order to illustrate the link with the seal shape.

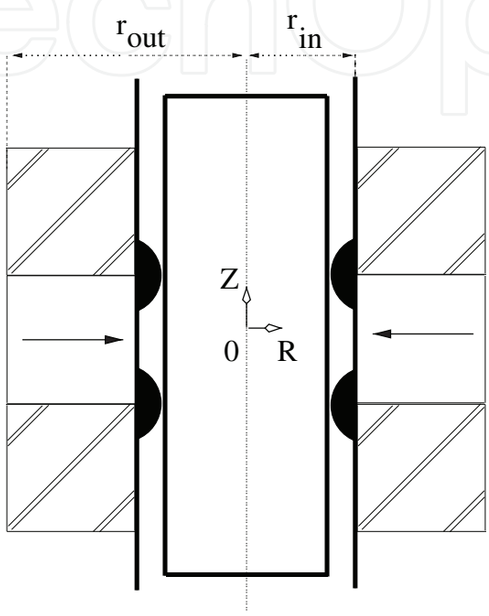

Fig. 5. Basic structure: three outer rings (permanent magnet or non-magnetic) radially centered forming an air gap with an inner non-magnetic piston. Ferrofluid seals located in the air gap. $r_{in} = 25mm$, $r_{out} = 28mm$.

5.2 Single magnet structures

The first structure considered corresponds exactly to the configuration shown in Fig.5, which is the simplest one which can be used. All the rings have the same square cross-section with a 3 mm side. The middle ring is a radially polarized permanent magnet and the upper and lower rings are non-magnetic. The magnetic field created by the magnet in the air gap is calculated along the Z axis at a 0.1 mm distance from the rings and its radial component H_r is plotted versus Z (Fig.7). As a remark, H_r is rather uniform in front of the magnet and two gradients are oberved in front of the magnet edges. Besides, the magnetic pressure in the air gap is calculated and plotted on Fig.6 as well: the iso-pressure lines determine the seal contour, its size depends on the ferrofluid quantity. Indeed, the ferrofluid goes in the regions of high energy first (dark red ones). For an increasing volume of ferrofluid, the latter fills the regions of decreasing energy (from the red contours to the blue ones). So, for seals thicker than 0.5 mm, the seal expands along the whole magnet height. A smaller volume of ferrofluid would lead to the creation of two separate seals which would be quite thin and thus, to poor mechanical properties. This results from the shape of the magnet section: if it were rectangular along Z instead of square, two separate seals would appear too. The point is that the ferrofluid seeks the regions of both intense field gradient and high magnetic energy.

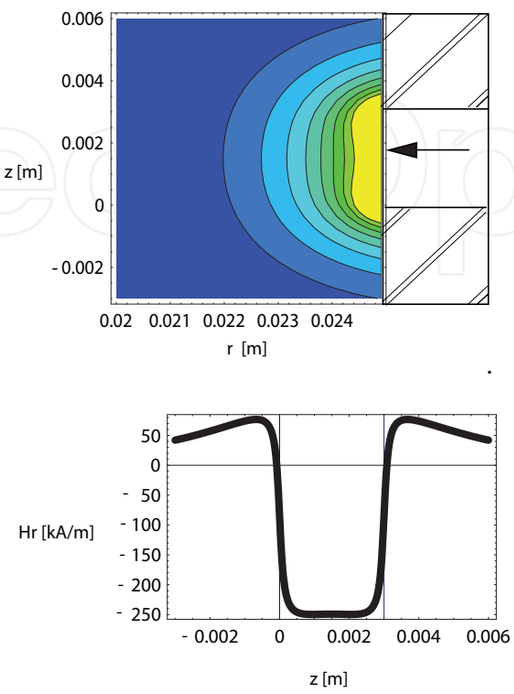

Fig. 6. Top right: upper and lower non-magnetic rings, middle ring permanent magnet radially polarized. Top left: magnetic pressure in front of the rings. Bottom: H_r along the Z axis at a 0.1 mm distance from the rings.

If the polarization direction of the ring magnet becomes axial, Fig. 7 shows that the magnetic pressure is at first sight rather similar to the previous one. Nevertheless, the seal shape differs, especially for large ferrofluid volumes. Moreover, the radial component of the magnetic field is no longer uniform in front of the magnet and presents instead a rather large gradient all over the magnet length and the non-magnetic rings.

5.3 Double magnet structures

The purpose is to describe how the seal shape and properties evolve when the magnetic structure becomes gradually more complicated but also maybe more efficient.

Then the structures considered are obtained by stacking two ring permanent magnets. The rings are identical in dimensions but are opposedly polarized, either radially as in Fig. 9 or axially as in Fig. 8. The magnetic field in both cases is evaluated by superposing the single magnet fields.

As a consequence, each radial magnet creates a region of uniform field in front of itself and the field directions are opposite. The field intensity in each uniform region is higher than in the single magnet structure because the leakage is decreased. Then, three field gradients exist, and the one that appears in front of the magnets' interface is twice as high as those at the edges. From the gradient point of view, Fig. 9 can be compared with Fig. 6, and the former will prove more useful because the gradient is steeper. The axial double structure creates progressive field gradients with no peculiar interest.

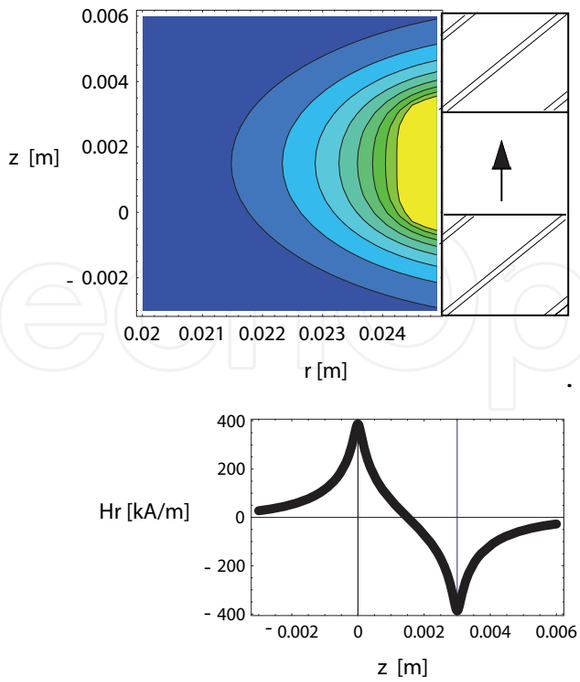

Fig. 7. Top right: upper and lower non-magnetic rings, middle ring permanent magnet axially polarized. Top left: magnetic pressure in front of the rings. Bottom: H_r along the Z axis at a 0.1 mm distance from the rings.

Moreover, the repartition of the magnetic energy density in the double magnet structure is not the superposition of the ones in the single magnet structures because the expression of the energy depends on the square of the field. Although the repartitions for radial and axial magnets seem alike at first sight, the radial structure is "more energetic" and its magnetic energy decreases slower at an increasing distance from the magnets. Nevertheless, the maximum energy density is in front of the magnets' interface and the ferrofluid seal will be located there. Eventually, the seal axial length in the single magnet structures is smaller than in the double magnet structures. Besides, the seal energy density is approximately doubled for the radially polarized magnets.
The evolution of the magnet shape can be observed when the axial dimension of the ring magnet is varied. For instance, Fig 10 shows the magnetic iso-pressure lines when both magnet heights are $h = 2$ mm, $h = 2.5$ mm , $h = 3$ mm, $h = 3.5$ mm, $h = 4$ mm and $h = 4.5$ mm respectively.
As expected, the magnetic field in the air gap increases when the magnet height increases. Figure 10 clearly shows that the longer the ring permanent magnet heights are, the stronger the magnetic field in the air gap is. However, as shown in Fig 10, the ferrofluid seal decreases in height when the ring permanent magnet heights increase. This implies that for a structure that requires a small ferrofluid seal with the greatest static capacity, the height of the ring permanent magnets must be greater than their radial widths.

5.4 Triple magnet structures

With the same reasoning as in previous section, the structures presented here are constituted of three stacked ring permanent magnets. Thus, the number of possible configurations increases. However, it isn't necessary to study all possibilities and the most interesting ones

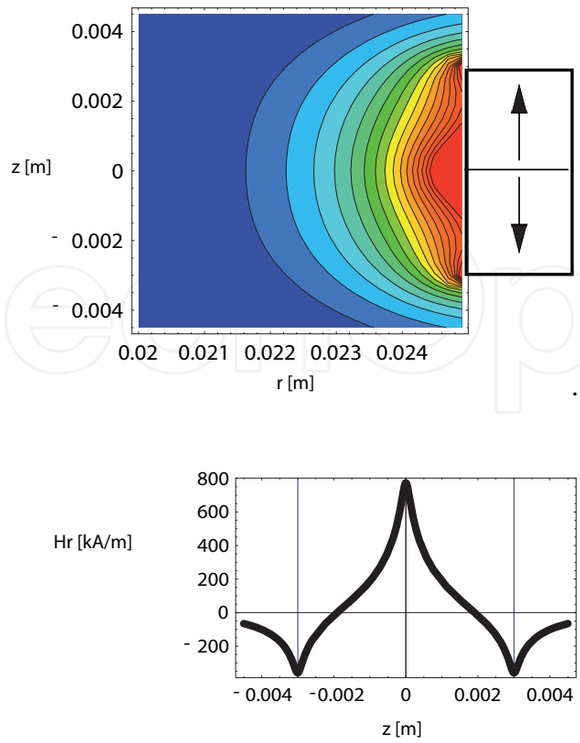

Fig. 8. Top right: Two ring permanent magnets with opposed axial polarization. Top left: magnetic pressure in front of the rings. Bottom: H_r along the Z axis at a 0.1 mm distance from the rings.

have been selected. Then, two main kinds of structures are brought out: structures with alternate polarizations and structures with rotating polarizations.

5.4.1 Alternate polarizations

The three rings are radially polarized: two have the same polarization direction, the third has the opposite direction and is located between both previous ones. Thus, this structure is the extension of the preceding double magnet structure, which can be generalized to even more ring magnets. Now, in the case of three ring magnets, the number of seals and their shape is closely related to the middle magnet axial height an to the ferrofluid total volume (Fig 11)
Indeed, the left top plot in Fig 11 shows that for three magnets of same dimensions and a small amount of ferrofluid, two seals are formed in front of the ring interfaces. Their axial dimension is rather small and they are very energetic. When the middle magnet height is decreased both seals get closer and join to form a single seal in front of the middle magnet. This seal is less energetic: it is normal as the middle magnet volume is decreased. Meanwhile, two secondary small seals appear at the extremities of the structure.
For a larger ferrofluid volume, a single seal is formed in front of the whole structure whatever the middle magnet dimensions and its energy is linked to the total magnet volume.

5.4.2 Rotating polarizations

The three ring magnets polarization directions are now alternately axial and radial and a 90 degrees rotation is observed from one magnet to its neighbor. Such a progressive rotation of the magnetic polarization is to put together with Halbach patterns (34).

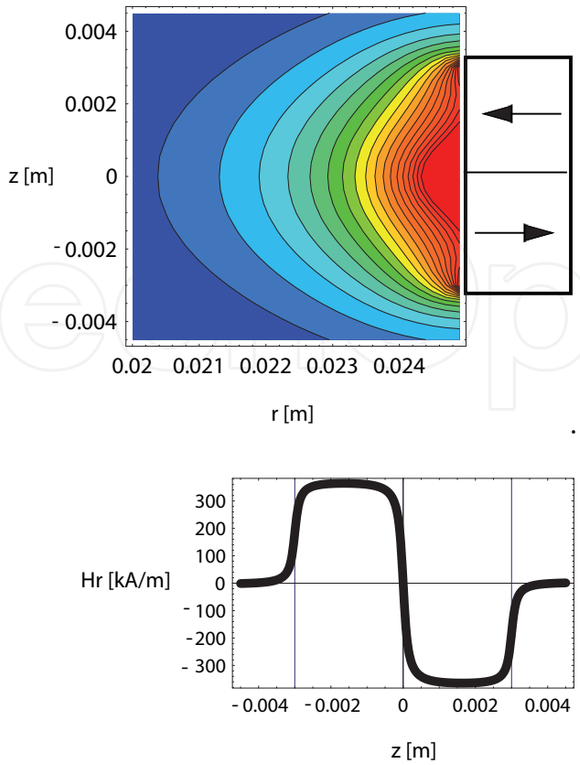

Fig. 9. Top right: Two ring permanent magnets with opposed radial polarization. Top left: magnetic pressure in front of the rings. Bottom: H_r along the Z axis at a 0.1 mm distance from the rings.

Two kinds of configurations are possible with three ring magnets: either two top and bottom axially and one middle radially polarized rings (Fig. 12) or the dual two top and bottom radially and one middle axially polarized rings (Fig. 13).
The energy density color plots show that two ferrofluid seals form in front of the magnets' interfaces. Their shape is rather similar in both structures and these seals are magnetically quite energetic. So, they will have "good" mechanical properties (such as a great radial stiffness for example). However, the magnetic field radial component proves different in each structure: it is fairly uniform in front of the middle radially polarized magnet whereas it varies with no particularly interesting properties in in front of the axially polarized one. As a consequence, the structure of Fig. 12 seams to be more useful for applications as the zone of uniform magnetic field can be optimized.
Indeed, the axial height of the middle magnet can be varied. For instance, the middle magnet is twice as high as each other magnet in Fig. 14 and half as small in Fig. 15. As a result, the magnetic field radial component is always rather uniform in front of the radially polarized magnet. So, the uniformity area increases with the height of the radially polarized magnet, but the field intensity decreases when the height of the radially polarized magnet is larger than the height of the axially polarized ones. Besides, when the height of the axially polarized magnets becomes too small the ferrofluid tends to expand over their whole axial length if the ferrofluid volume is sufficient. Thus, the seals can become quite large and they are well-fixed to the structure and have high mechanical performances because of their high magnetic energy and the steep field gradients.

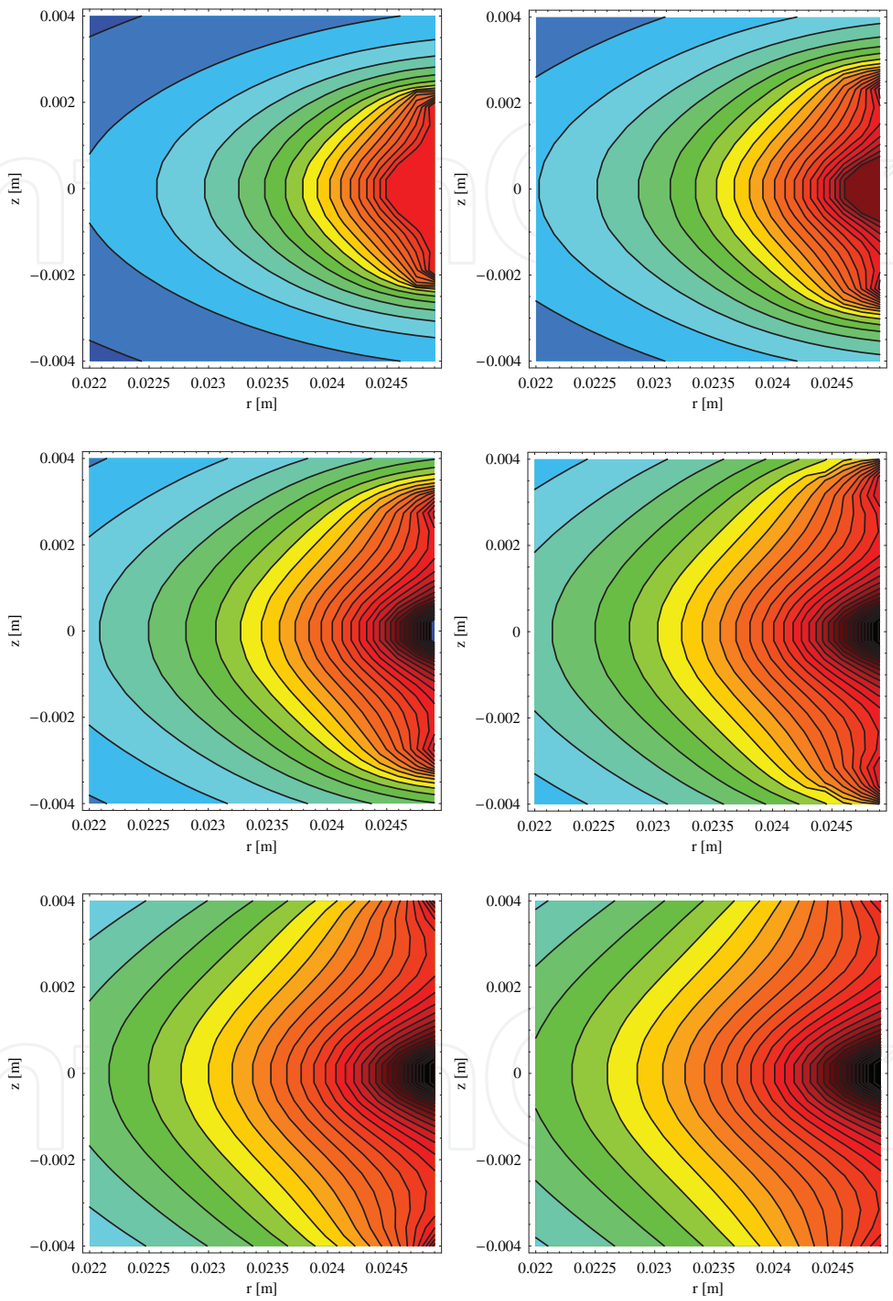

Fig. 10. Magnetic iso-pressure lines for increasing ring magnet heights; $h = 2$ mm (top left), $h = 2.5$ mm (top right), $h = 3$ mm (middle left), $h = 3.5$ mm (middle right), $h = 4$ mm (bottom left), $h = 4.5$ mm (bottom right).

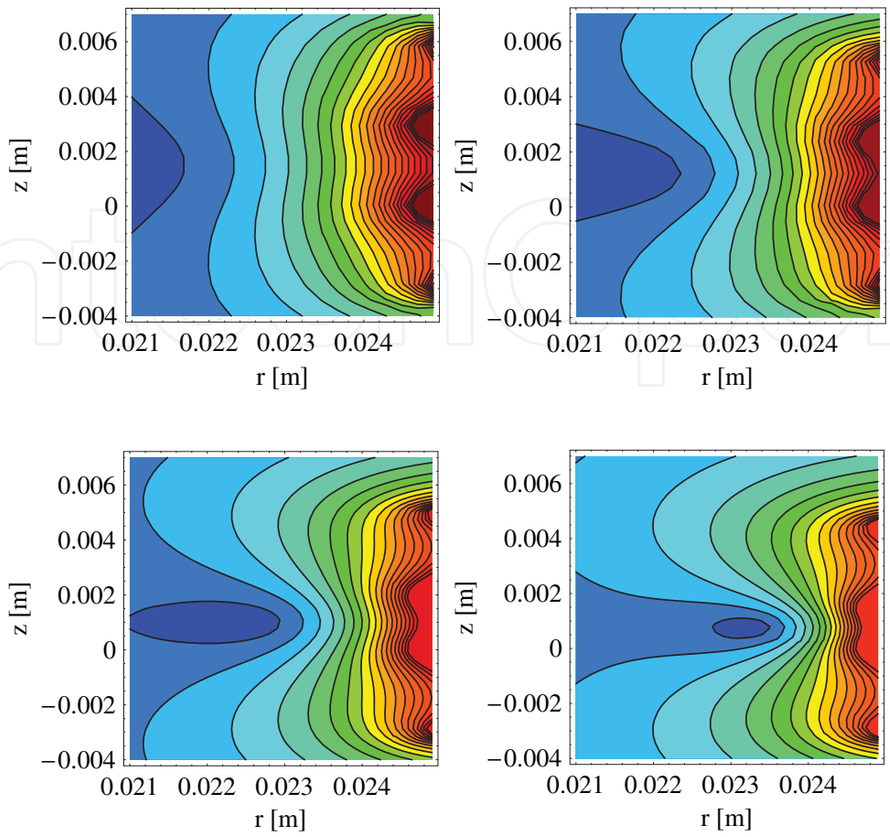

Fig. 11. Three magnet alternate structure. Magnetic iso-pressure lines in the air gap for a decreasing height of the middle magnet $h = 3$ mm, $h = 2.5$ mm, $h = 2$ mm, $h = 1.5$ mm.

Inversely, when the middle radially polarized magnet height becomes too small, both seals gather to form a single high energetic one which expands over the whole height of the middle magnet.

6. Mathematical description of the ferrofluid seal

Writing the whole mathematical equations describing all the ferrofluid properties doesn't lead to easily workable expressions. This exercise is still very complicated even if the only equations considered are the ones related to the magnetic pressure. Nevertheless, in the double magnet structure with radially polarized ring magnets, the seal shape can be described in a very good approximation by an equation of ellipse.
This allows some further characterization of the seal and especially its behavior when it gets crushed and works as a bearing.

6.1 Shape of the free ferrofluid seal

This section considers the shape of the seal when its boundary surface is totally free, so in absence of the inner moving part or for volumes small enough not to reach the inner part.

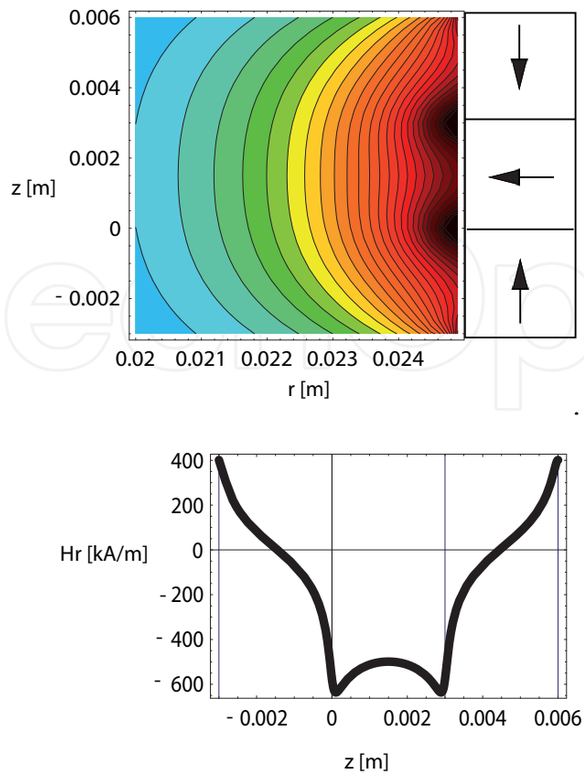

Fig. 12. Top right: axially polarized upper and lower rings, radially polarized middle ring. Top left: magnetic pressure in front of the rings. Bottom: H_r along the Z axis at a 0.1 mm distance from the rings.

Ellipse	a_i	b_i	r_i	error
5%E	0.00025	0.000275	0.025	0.5%
10%E	0.00027	0.000297	0.025	0.9%
15%E	0.00029	0.000319	0.025	1.4%

Table 2. Parameters describing the free boundary ferrofluid seal shape.

For example, the contour of the ferrofluid seal in Fig 16 when its thickness is smaller than 0.4 mm can be written in terms of the following equation of an ellipse (21).

$$\frac{(r-r_i)^2}{a_i^2}+\frac{z^2}{b_i^2}=1 \tag{21}$$

The parameter values are given in Table (2) when r is between 24.6 mm and 25 mm. Moreover, E is the total magnetic energy of the volume of ferrofluid located between 24.6 mm and 25 mm. Table (2) shows the proportion of energy located in the seal of considered dimensions. The error between the equations of ellipse and the real contour shape of the ferrofluid seal is also given.
When the ferrofluid volume increases and the seal goes further than $r = 24.6$ mm towards the axis, its shape changes and is no longer a portion of an ellipse. This gives the limits of our

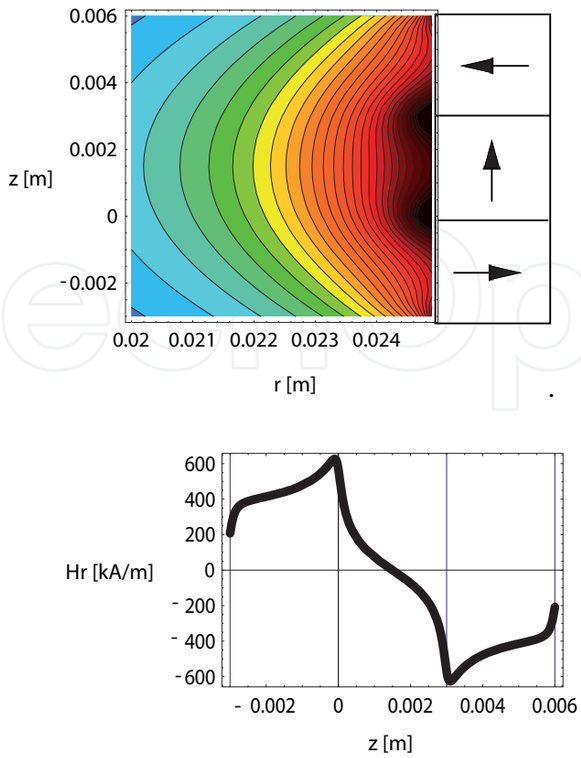

Fig. 13. Top right: radially polarized upper and lower rings, axially polarized middle ring. Top left: magnetic pressure in front of the rings. Bottom: H_r along the Z axis at a 0.1 mm distance from the rings.

modelling. However, it can be noted that the most energetic seals are the ones whose contour remain a portion of an ellipse.

6.2 Shape of the crushed ferrofluid seal

So, the model can be used further to describe the seal in presence of the inner moving part. As previously said, this part is a non magnetic cylinder forming an air gap with the permanent magnet structure. The device dimensions and the ferrofluid volume are chosen so that the seal plays its watertightening role. This means that the seal is crushed by the inner part (Fig.17). The point is that for adequate ferrofluid volumes, the ferrofluid seal contour can still be described in terms of an equation of ellipse.

If the same ferrofluid volume is considered as in the previous section, then adding the inner part results in the fact that the ferrofluid volume can't remain in the radial space and is driven away in the axial direction towards the free space of the air gap. As the geometry is axisymmetrical, the new seal contour is symmetrical and can be described as a truncated ellipse (Fig. 17).

The point is that when the seal shape changes because it is crushed its magnetic energy decreases. This is illustrated by the values of Table 3 which present the energy reduction when the inner cylinder radius grows of respectively $0,1$ mm, $0,15$ mm and $0,2$ mm. This is of importance as the seal properties or performances are directly related to its magnetic energy.

It can be noted that a 0.2 mm increase of the inner cylinder radius causes a 68% energy reduction.

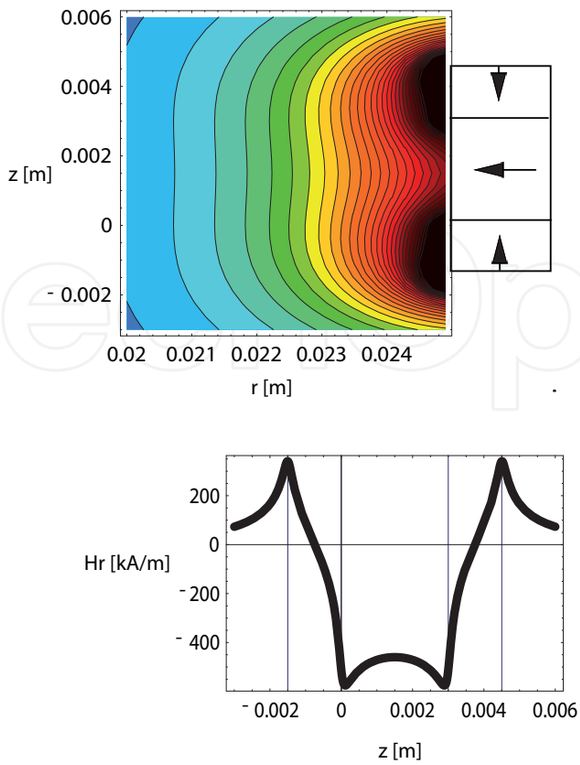

Fig. 14. Top right: axially polarized upper and lower rings, radially polarized middle ring, the axial magnet height is the half of the radial magnet one. Top left: magnetic pressure in front of the rings. Bottom: H_r along the Z axis at a 0.1 mm distance from the rings.

Radius increase	Energy reduction
0, 1 mm	13%
0, 15 mm	35%
0, 2 mm	68%

Table 3. The inner cylinder radius increase causes an energy reduction in the seal.

This modelling is useful to evaluate the mechanical properties and performances of ferrofluid seals.

7. Capacity of the ferrofluid seal

The static capacity of the ferrofluid seals is an important characteristic as it determines the maximal axial pressure they can undergo without losing their tightness property. It depends naturally on the chosen configuration and this issue will be discussed later on.
In some applications, the pressures on each side of the seal can be pretty different. Consequently, a pressure gradient appears: the ferrofluid seal is deformed and can be pierced (or blown) along the moving part for too high pressures. Therefore, the knowledge of the seal capacity is necessary or, inversely, the seal may be dimensionned to have a given capacity.
So, the configuration considered for the calculation corresponds to the case when a cylindrical air gap appears in the seal along the cylinder because of an applied pressure on one side of the seal (Fig.18).

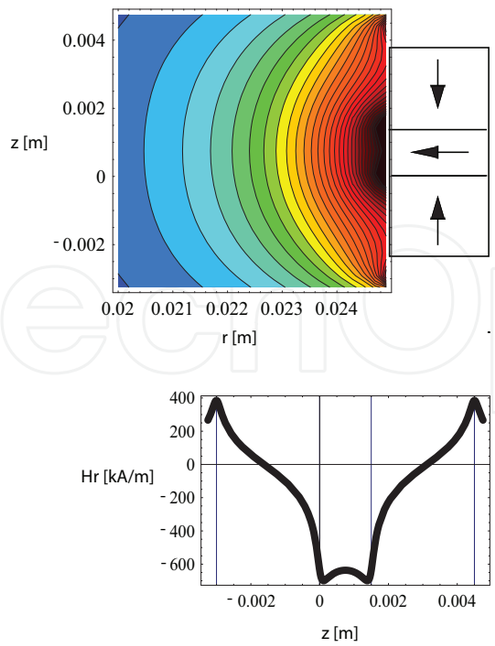

Fig. 15. Top right: axially polarized upper and lower rings, radially polarized middle ring, the axial magnet height is the double of the radial magnet one. Top left: magnetic pressure in front of the rings. Bottom: H_r along the Z axis at a 0.1 mm distance from the rings.

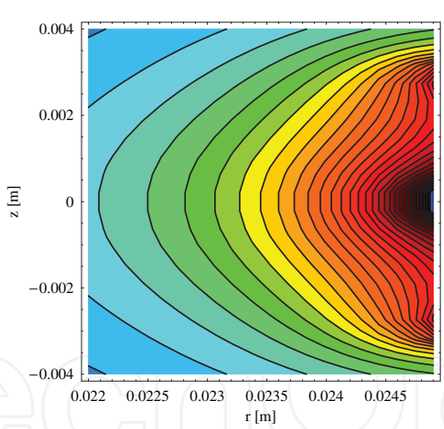

Fig. 16. Magnetic iso-pressure lines for $h = 3$ mm.

The ferrofluid seal capacity is determined in two steps. First, the potential energy of the ferrofluid seal is evaluated without any hole in the seal. The numerical integration of (24) leads to a first value of the potential energy, $E_m(1)$. Second, the potential energy, $E_m(2)$, of the ferrofluid seal with the hole is evaluated with another numerical integration. The energy difference, ΔE_m, corresponds to the pressure work $\delta W(P)$ and satisfies (22):

$$\Delta E_m = E_m(1) - E_m(2) = \delta W(P) = P_{lim} S d \tag{22}$$

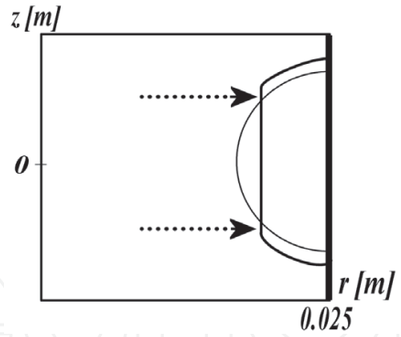

Fig. 17. Crushed ferrofluid seal.

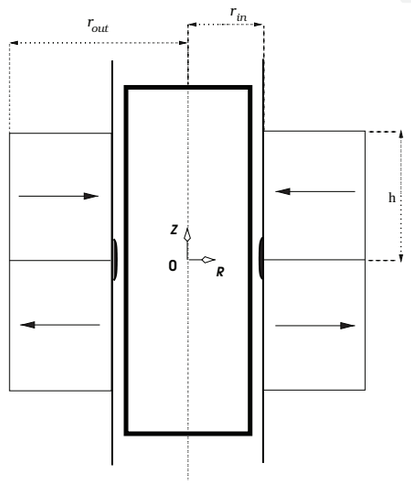

Fig. 18. Seal pierced along the inner cylinder.

Seal thickness	**Volume**	H_{lim}
0, 1 mm	4.7 mm^3	700 000 A/m
0, 3 mm	12 mm^3	600 000 A/m
0, 5 mm	21 mm^3	450 000 A/m

Table 4. Seal volume and Magnetic field for a given ferrofluid seal thickness

where S is the surface of the air gap and d is the thickness of the hole. Consequently, the capacity P_{lim} is given by (23):

$$P_{lim} = \frac{\delta W(P)}{Sd} \tag{23}$$

Numerical values have been calculated with several ring inner radii and are shown on Fig.19 where the ferrofluid seal thickness is defined as the axial thickness of the ferrofluid in the air gap.
Figure 19 also illustrates that thin ferrofluid seals resist to higher pressure gradients than thick ones. Besides, Table 4 gives the ferrofluid volume corresponding to each seal thickness and the lowest magnetic field H_{lim} in the seal volume.

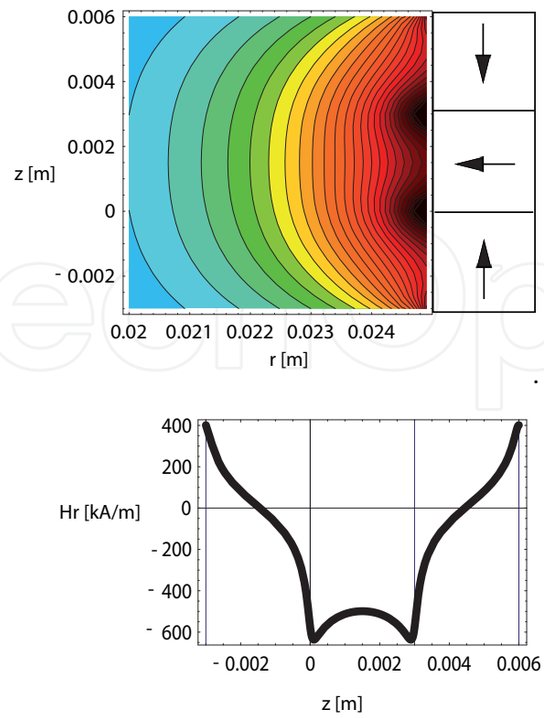

Fig. 19. The static capacity P_{lim}[Pa] of the ferrofluid seal depends on its thickness $ft[mm]$

8. Ferrofluid seals as bearings

One of the issues of the use of ferrofluid seals is their behavior as radial bearings. Indeed, when the inner moving part is no longer radially centered the ferrofluid seal exerts a pull back centering force and the corresponding radial stiffness can be evaluated.

8.1 Radial stiffness evaluation

The considered position of the inner moving part is illustrated both on Fig.20 and Fig.21.

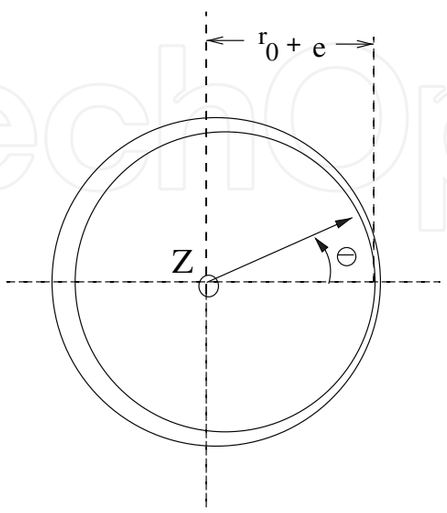

Fig. 20. Decentered inner cylinder: cross-section.

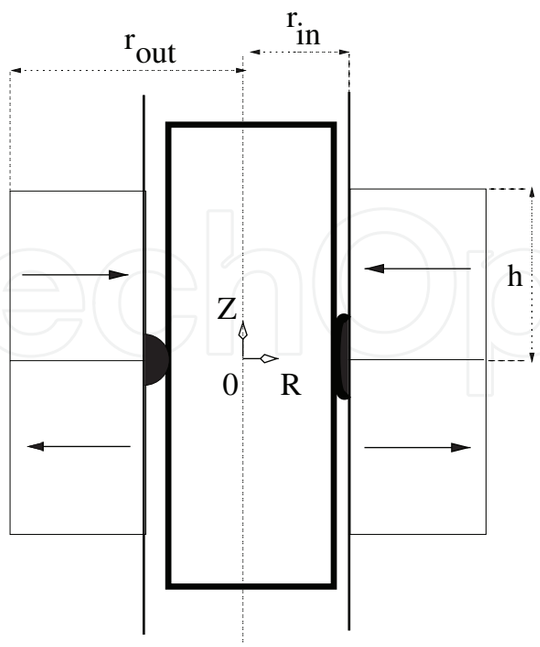

Fig. 21. Decentered inner cylinder: crushed ferrofluid.

They show that the air gap radial dimension depends on the angle θ. Moreover, the problem is now fully three-dimensional. Indeed, when the inner cylinder moves radially, the ferrofluid is more crushed on the narrow air gap side and it is driven away not only in the axial direction but also around the inner cylinder towards the regions of broader airgap. The new ferrofluid repartition is achieved according to energy considerations.
The evaluation of the radial stiffness is carried out in two steps.
First, the potential energy $E_m(1)$ is calculated when the non-magnetic cylinder is centered (Fig.1) with (24):

$$E_m = -\int\int\int_{(\Omega)} p_m(r,z)dV \tag{24}$$

Then, the potential energy $E_m(2)$ is calculated when the non-magnetic cylinder is decentered (Fig.21). In this second configuration, the limits of the integrals depend on the angle θ. Thus, the potential energy $E_m(2)$ is determined with (25):

$$E_m(2) = \int_0^{2\pi}\int_{r_0+e\cos(\theta)}^{r_{in}}\int_{-z_0}^{z_0} e_m(r,z)rdrd\theta dz \tag{25}$$

where r_0 and e are determined by the equation of the decentered circle (26):

$$r(\theta) = r_0 + e\cos(\theta) \tag{26}$$

where $r_0 = 24.7$ mm and $e = 0.1$ mm.
The radial force F_r is then calculated with (27):

$$F_r = \frac{E_m(1) - E_m(2)}{2\Delta r} \tag{27}$$

where $\Delta r = 1$ mm is the radial decentering of the inner cylinder.

Eventually, the radial stiffness k_r is determined by (28):

$$k_r = \frac{F_r}{\Delta r} \tag{28}$$

As a result, the numerical value of the radial stiffness is $k_r = 5.6$ N/mm for a ferrofluid seal of 0.3 mm thickness.

9. Comments and discussion

Thus far, this chapter described how ferrofluid seals are formed in magnetic structures and which shape and characteristics they have. Now, this section intends to comment and compare these structures with regard to the seals properties and performances in relation with the intended kind of application.
Indeed, the design depends on the goal and two major trends can be highlighted: the application consists in creating a seal for tightness purposes only or it intends to create a seal and a useful magnetic field, as in voice coil motors for example.

9.1 General purpose

In each case the seal mechanical properties are one of the issues, if not the only one.
Now, the structures presented can be very simple or more elaborate. Of course, the simplest ones are the single magnet structures, which lead to rather similar seals whatever the polarization direction. However, axially polarized ring magnets are cheaper and more easily available than radially polarized ones because the axial polarization is technically far easier to achieve. So, for simple and cheap solutions the choice should be a single axially polarized ring magnet.
Though, the mechanical robustness of the seal is linked to the magnetic pressure and the magnetic potential energy in the seal. Therefore, the high performance structures are not the simplest ones. Indeed, the previous sections show that multi-magnet structures create higher magnetic fields as well as larger field gradients to trap and fix the ferrofluid and that the thus formed seals are in areas of higher magnetic pressure.
The air gap dimensions can be chosen but must fulfill mechanical constraints: the movement of the inner part must be possible with the known mechanical clearances, the machining tolerances of the parts must be taken into account...Besides, the performances of a ferrofluid seal depend on the magnetic structure dimensions and on the seal thickness. For instance, the triple magnet structures of Fig. 15 or Fig. 12 lead to efficient seals thinner than the double magnet structures of Fig. 9 because the region of high magnetic pressure is radially thinner. Then, for given air gap dimensions, the type of magnetic structure is chosen with regard to the intended class of performances (low or high...) and then the ferrofluid volume is determined to achieve the optimal properties for this structure. And the ferrofluid shape depends on both the magnetic pressure and the ferrofluid volume.
Furthermore, “optimal properties” often means that the seal is robust and can resist rather high axial pressures, so, that its capacity is high. The preceding sections have shown that this is the case when the seal exerts an opposing force, related itself to energy variations in the ferrofluid seal. A great energy variation creates a high intensity force. Therefore, a high capacity is achieved when the iso-pressure lines are very close together in the axial direction: the energy variation will be large for axial displacements of the seal contour thus creating a considerable force. The preceding calculations and their illustrations show that thin seals are more energetic. Then, if a thin seal must achieve the tightness the air gap should be rather thin either. But the notion of “thin air gap” or “thin seal” is a relative one, defined in fact

with regard to the magnetic structure axial dimension. Indeed, in the taken examples a thin seal corresponds to a seal whose radial dimension is around the tenth of a ring magnet axial thickness. So, the seal can be the twentieth or the thirtieth of the axial total dimension for multi-magnets devices. And the axial dimension of the magnets is a tunable parameter.
As shown in Fig 10, the ferrofluid seal axial height decreases when the ring magnet height increases. This implies that for a structure that requires an axially narrow ferrofluid seal with a high static capacity, the height of the ring magnets must be larger than their radial width.
Moreover, the radial magnet dimension can also be tuned to achieve a high static capacity. Indeed, if the radial dimension is increased, the magnetic field intensity in the air gap is increased and so is the potential energy.
Thus, the design will generally be the result of trade-offs and the modelling presented will greatly help the device dimensioning and optimizing.
As the seal has a radial bearing behavior too, it must be characterized with regard to this function. So, the maximal radial decentering without creation of a hole in the seal for a given ferrofluid volume has to be determined. This can also be evaluated thanks to the presented modelling. For example, for a ferrofluid volume corresponding to a free boundary seal of 0.4 mm radial thickness and an inner moving part creating a 0.3 mm wide air gap, the maximal radial displacement of the moving part without tightness loss is 0.14 mm (ring magnets dimensions: $r_{in} = 25$ mm, $r_{out} = 28$ mm, $h = 3$ mm).

9.2 Special applications: transducers

Now, if the created magnetic field itself is of importance, like in actuators or sensors, the intensity and the uniformity of the field in the air gap are additionnal issues.
Indeed, voice coil motors require the creation of a force which is as exactly as possible the image of the driving current. This can be achieved if the magnetic field created by the permanent magnets and applied to the coil is uniform. Moreover, the efficiency is proportionnal to the field level.
These requirements are the same in transducers like seismometers, in which ferrofluid seals can be used as bearings and guiding systems. But, the field level will characterize the sensor sensitivity rather than an efficiency.
And they are even more important in special voice coil motors such as loudspeakers, in which the ferrofluid seal is used to ensure the airtightness, to transfer the heat from the moving part to the steady one, to work as a radial bearing and to replace the loudspeaker suspension thus contributing to the improvement of the loudspeaker linearity. Therefore, the structures presented in Figs. 5, 9 and 12 with radialy magnetized magnets and creating uniform magnetic field radial components are the most useful for loudspeaker appications. The triple magnet structures, though more complicated, offer the possibility of a multi-criteria optimization which will make the design easier and is enabled by the proposed analytical formulations and modelling.

10. Conclusion

Thus this chapter presents how ferrofluids can be used to form seals in various ironless magnetic structures. As preamble, the analytical evaluation of the magnetic field created by ring permanent magnets is given. Then, a simple analytical model is proposed to describe the static behavior of the ferrofluid seals: their shape, their static capacity, their working as bearings.
The originality of the considered structures lies in the fact that they are made of permanent magnet only, without any iron on the static part nor on the moving part which is a non magnetic cylinder.

Various magnetic structures are presented: some are very simple with a single ring magnet, some more complicated with three ring magnets. For each of them, the forming of one or more ferrofluid seal is decribed, with regard to the magnetic structure geometry and the ferrofluid volume. The properties and performances of the seals are also characterized and compared thanks to the concepts of magnetic pressure and magnetic potential energy. The modelling proves to be very useful and efficient to illustrate the magnet role and deduct design rules for ferrofluid seals with given mechanical characteristics.
Some information is also given for peculiar application such as voice coils motors in which the magnetic structure plays the double role of fixing the ferrofluid seal and creating a magnetic field with special properties such as uniformity.

11. References

[1] J. Bajkowski, J. Nachman, M. Shillor, and M. Sofonea, "A model for a magnetorheological damper," *Mathematical and computer modelling*, vol. 48, pp. 56–68, 2008.
[2] R. E. Rosensweig, *Ferrohydrodynamics*. Dover, 1997.
[3] O. Doutres, N. Dauchez, J. M. Genevaux, and G. Lemarquand, "On the use of a loudspeaker for measuring the viscoelastic properties of sound absorbing materials," *Journal of the Acoustical Society of America Express Letters*, vol. 124, no. 6, pp. EL335–EL340, 2008.
[4] X. Li, K. Yao, and Z. Liu, "Cfd study on the magnetic fluid delivering in the vessel in high-gradient magnetic fields," *Journal of Magnetism and Magnetic Materials*, vol. 320, pp. 1753–1758, 2008.
[5] G. S. Park and K. Seo, "New design of the magnetic fluid linear pump to reduce the discontinuities of the pumping forces," *IEEE Trans. Magn.*, vol. 40, pp. 916–919, 2004.
[6] I. Tarapov, "Movement of a magnetizable fluid in lubricating layer of a cylindrical bearing," *Magnetohydrodynamics*, vol. 8, no. 4, pp. 444–448, 1972.
[7] R. C. Shah and M. Bhat, "Ferrofluid squeeze film in a long bearing," *Tribology International*, vol. 37, pp. 441–446, 2004.
[8] S. Chen, Q. Zhang, H. Chong, T. Komatsu, and C. Kang, "Some design and prototyping issues on a 20 krpm hdd spindle motor with a ferro-fluid bearing system," *IEEE Trans. Magn.*, vol. 37, no. 2, pp. 805–809, 2001.
[9] Q. Zhang, S. Chen, S. Winoto, and E. Ong, "Design of high-speed magnetic fluid bearing spindle motor," *IEEE Trans. Magn.*, vol. 37, no. 4, pp. 2647–2650, 2001.
[10] P. Kuzhir, "Free boundary of lubricant film in ferrofluid journal bearings," *Tribology International*, vol. 41, pp. 256–268, 2008.
[11] M. Miwa, H. Harita, T. Nishigami, R. Kaneko, and H. Unozawa, "Frequency characteristics of stiffness and damping effect of a ferrofluid bearing," *Tribology Letter*, vol. 15, no. 2, pp. 97–105, 2003.
[12] W. Ochonski, "The attraction of ferrofluid bearings," *Mach. Des.*, vol. 77, no. 21, pp. 96–102, 2005.
[13] Z. Meng and Z. Jibin, "An analysis on the magnetic fluid seal capacity," *Journal of Magnetism and Magnetic Materials*, vol. 303, pp. e428–e431, 2006.
[14] J. Walker and J. Backmaster, "Ferrohydrodynamics thrust bearings," *Int. J. Eng. Sci.*, vol. 17, pp. 1171–1182, 1979.
[15] N. Tiperi, "Overall characteristics of bearings lubricated ferrofluids," *ASME J. Lubr. Technol.*, vol. 105, pp. 466–475, 1983.
[16] S. Miyake and S. Takahashi, "Sliding bearing lubricated with ferromagnetic fluid," *ASLE Trans.*, vol. 28, pp. 461–466, 1985.

[17] H. Chang, C. Chi, and P. Zhao, "A theoretical and experimental study of ferrofluid lubricated four-pocket journal bearing," *Journal of Magnetism and Magnetic Materials*, vol. 65, pp. 372–374, 1987.
[18] Y. Zhang, "Static characteristics of magnetized journal bearing lubricated with ferrofluids," *ASME J. Tribol.*, vol. 113, pp. 533–538, 1991.
[19] T. Osman, G. Nada, and Z. Safar, "Static and dynamic characteristics of magnetized journal bearings lubricated with ferrofluid," *Tribology International*, vol. 34, pp. 369–380, 2001.
[20] R. C. Shah and M. Bhat, "Anisotropic permeable porous facing abd slip velocity squeeze film in axially undefined journal bearing with ferrofluid lubricant," *Journal of Magnetism and Magnetic Materials*, vol. 279, pp. 224–230, 2004.
[21] F. Cunha and H. Couto, "A new boundary integral formulation to describe three-dimensional motions of interfaces between magnetic fluids," *Applied mathematics and computation*, vol. 199, pp. 70–83, 2008.
[22] R. E. Rosensweig, Y. Hirota, S. Tsuda, and K. Raj, "Study of audio speakers containing ferrofluid," *J. Phys. : Condens. Matter*, vol. 20, 2008.
[23] G. Lemarquand, "Ironless loudspeakers," *IEEE Trans. Magn.*, vol. 43, no. 8, pp. 3371–3374, 2007.
[24] R. Ravaud and G. Lemarquand, "Modelling an ironless loudspeaker by using three-dimensional analytical approaches," *Prog. Electromagn. Res.*, vol. 91, pp. 53–68, 2009.
[25] R. Ravaud, G. Lemarquand, V. Lemarquand, and C. Depollier, "Ironless loudspeakers with ferrofluid seals," *Archives of Acoustics*, vol. 33, no. 4S, pp. 3–10, 2008.
[26] R. Ravaud, G. Lemarquand, and V. Lemarquand, "Magnetic pressure and shape of ferrofluid seals in cylindrical structures," *J. Appl. Phys.*, vol. 106, no. 3, p. 34911, 2009.
[27] R. Ravaud, M. Pinho, G. Lemarquand, N. Dauchez, J. M. Genevaux, V. Lemarquand, and B. Brouard, "Radial stiffness of a ferrofluid seal," *IEEE Trans. Magn.*, vol. 45, no. 10, pp. 4388–4390, 2009.
[28] R. Ravaud, G. Lemarquand, and V. Lemarquand, "Mechanical properties of ferrofluid applications: centering effect and capacity of a seal," *Tribology International*, vol. 43, no. 1-2, pp. 76–82, 2009.
[29] A. Ivanov, S. Kantorovich, V. Mendelev, and E. Pyanzina, "Ferrofluid aggregation in chains under the influence of a magnetic field," *Journal of Magnetism and Magnetic Materials*, vol. 300, pp. e206–e209, 2006.
[30] S. I. Babic and C. Akyel, "Improvement in the analytical calculation of the magnetic field produced by permanent magnet rings," *Prog. Electromagn. Res. C*, vol. 5, pp. 71–82, 2008.
[31] R. Ravaud, G. Lemarquand, and V. Lemarquand, "Magnetic field created by tile permanent magnets," *IEEE Trans. Magn.*, vol. 45, no. 7, pp. 2920–2926, 2009.
[32] R. Ravaud and G. Lemarquand, "Comparison of the coulombian and amperian current models for calculating the magnetic field produced by arc-shaped permanent magnets radially magnetized," *Prog. Electromagn. Res.*, vol. 95, pp. 309–327, 2009.
[33] R. Ravaud, G. Lemarquand, V. Lemarquand, and C. Depollier, "The three exact components of the magnetic field created by a radially magnetized tile permanent magnet.," *Prog. Electromagn. Res.*, vol. 88, pp. 307–319, 2008.
[34] K. Halbach, "Design of permanent multiple magnets with oriented rec material," *Nucl. Inst. Meth.*, vol. 169, pp. 1–10, 1980.

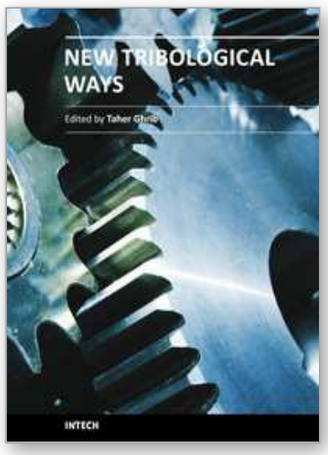

New Tribological Ways

Edited by Dr. Taher Ghrib

ISBN 978-953-307-206-7
Hard cover, 498 pages
Publisher InTech
Published online 26, April, 2011
Published in print edition April, 2011

This book aims to recapitulate old information's available and brings new information's that are with the fashion research on an atomic and nanometric scale in various fields by introducing several mathematical models to measure some parameters characterizing metals like the hydrodynamic elasticity coefficient, hardness, lubricant viscosity, viscosity coefficient, tensile strength .... It uses new measurement techniques very developed and nondestructive. Its principal distinctions of the other books, that it brings practical manners to model and to optimize the cutting process using various parameters and different techniques, namely, using water of high-velocity stream, tool with different form and radius, the cutting temperature effect, that can be measured with sufficient accuracy not only at a research lab and also with a theoretical forecast. This book aspire to minimize and eliminate the losses resulting from surfaces friction and wear which leads to a greater machining efficiency and to a better execution, fewer breakdowns and a significant saving. A great part is devoted to lubrication, of which the goal is to find the famous techniques using solid and liquid lubricant films applied for giving super low friction coefficients and improving the lubricant properties on surfaces.

How to reference

In order to correctly reference this scholarly work, feel free to copy and paste the following:

V. Lemarquand and G. Lemarquand (2011). Ferrofluid Seals, New Tribological Ways, Dr. Taher Ghrib (Ed.), ISBN: 978-953-307-206-7, InTech, Available from: http://www.intechopen.com/books/new-tribological-ways/ferrofluid-seals

INTECH
open science | open minds

InTech Europe
University Campus STeP Ri
Slavka Krautzeka 83/A
51000 Rijeka, Croatia
Phone: +385 (51) 770 447
Fax: +385 (51) 686 166
www.intechopen.com

InTech China
Unit 405, Office Block, Hotel Equatorial Shanghai
No.65, Yan An Road (West), Shanghai, 200040, China
中国上海市延安西路65号上海国际贵都大饭店办公楼405单元
Phone: +86-21-62489820
Fax: +86-21-62489821

© 2011 The Author(s). Licensee IntechOpen. This chapter is distributed under the terms of the Creative Commons Attribution-NonCommercial-ShareAlike-3.0 License, which permits use, distribution and reproduction for non-commercial purposes, provided the original is properly cited and derivative works building on this content are distributed under the same license.

IntechOpen

IntechOpen